Supplementary Information

Structure of the catalytic sites in Fe/N/C-catalysts for O_2-reduction in PEM fuel cells

Ulrike I. Kramm [a,b,*], Juan Herranz [a], Nicholas Larouche [a], Thomas M. Arruda [c], Michel Lefèvre [a],
Frédéric Jaouen [a], Peter Bogdanoff [b], Sebastian Fiechter [b], Irmgard Abs-Wurmbach [d],
Sanjeev Mukerjee [c], Jean-Pol Dodelet [a,*]

[a] Institut National de la Recherche Scientifique, Énergie, Matériaux et Télécommunications
Varennes, Québec, J3X 1S2, Canada

[b] Helmholtz-Zentrum Berlin für Materialen und Energie
Lise-Meitner-Campus, Institute for solar fuels and energy storage (E-I6)
Hahn-Meitner-Platz 1, D-14109, Berlin, Germany

[c] Northeastern University, Department of Chemistry and Chemical Biology,
317 Egan Research Center, 360 Huntington Avenue, Boston MA-02115, U.S.A

[d] Technical University Berlin, Faculty VI, Ackerstrasse 76, D-13355, Berlin, Germany

*Corresponding authors: Kramm@tu-cottbus.de; dodelet@emt.inrs.ca

Characterization Methods used in the Supplementary Information

X-ray diffraction measurements were made in order to check for any crystaline phases in the samples. The measurements were carried out employing a Bruker D8 Advance diffractometer in Bragg-Brentano Θ - 2Θ geometry, using Cu-K_α-radiation ($\lambda = 0.154$ nm). A Silicon disc was used as the sample holder, which was rotated during the measurements. Spectra were recorded in a 2Theta-region of $10° < 2\Theta < 60°$. The measured diffractograms were analyzed using the JCPDS database.

The specific surface area of all catalysts was derived from the BET analysis of their N_2-sorption isotherm (77 K), performed on a Quantachrome Autosorb-1 instrument. Their pore size distribution was determined with the Autosorb-1 software, using the quenched solid density functional theory (QSDFT) and assuming that the pores have a slit-like geometry. The surface area of micropores corresponds to that of pores having widths ≤ 2 nm; the mesoporous surface, to the difference between the total cumulative surface area and the microporous surface area; and the macroporous surface area, to the total BET minus the cumulative surface area.

Combustion analysis of the different catalysts was performed to determine their relative contents in nitrogen, carbon, hydrogen and sulphur. The measurements were performed by the group of Prof. Linker at the University of Potsdam with an Elementar Vario EL III analysis system.

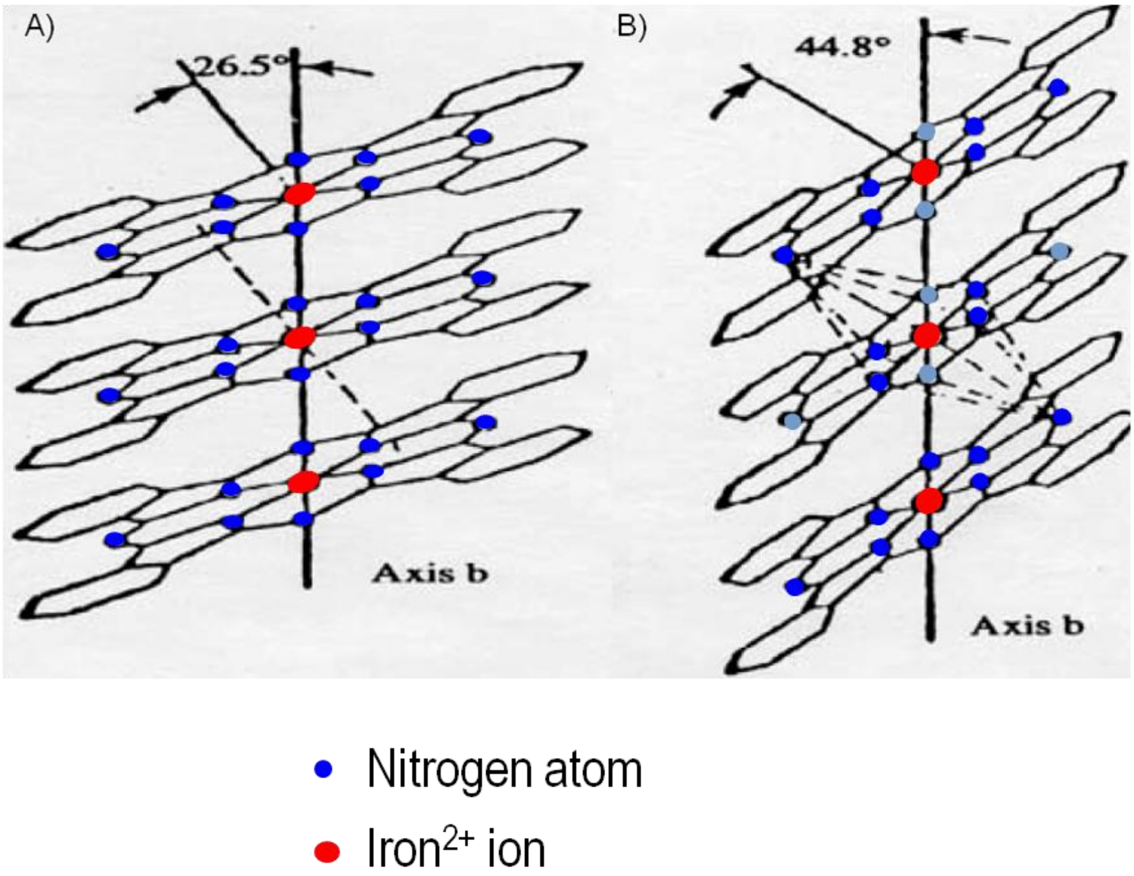

both: δ_{ISO}= 0.36 mm/s

α-FePc: ΔE_Q = 2.44 mm/s

β-FePc: ΔE_Q = 2.58 mm/s

Figure S1: Stacking of iron phthalocyanine molecules within the alpha- (A) and beta- (B) polymorphs of Fe-phthalocyanine. The figure was adapted from Figure 1 of ref. 1. In order to highlight the specific interactions of the Fe ion of the middle FePc molecule with the nitrogen atoms belonging to the FePc molecules above and below the middle one, the iron ions are painted in red and the nitrogen atoms in blue. While the isomer shift δ_{ISO} is similar for both polymorphs the quadrupole splitting ΔE_Q slightly changes induced by differences in the interactions.

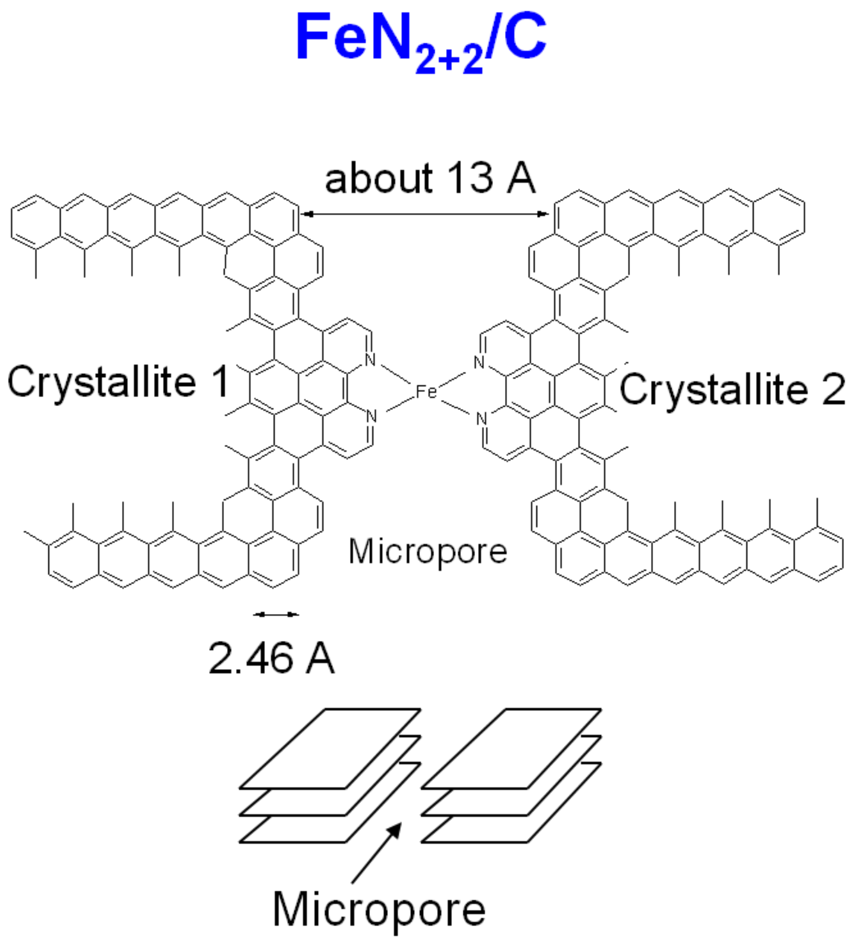

Figure S2: Possible structure of FeN_{2+2}/C as shown in Ref: 2

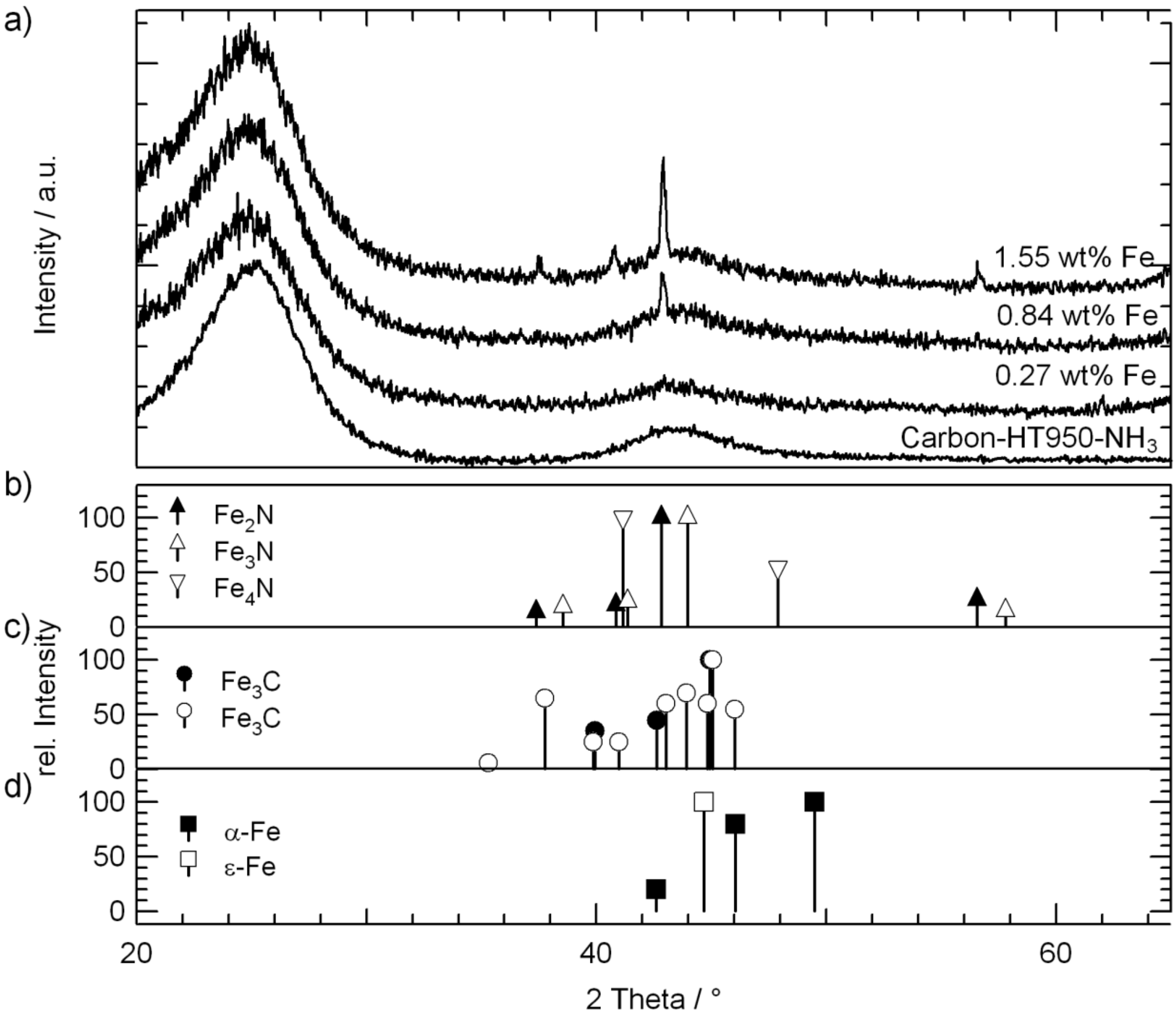

Figure S3: X-ray diffractograms of catalysts with different amounts of iron and, for comparison, of the Fe-free, ammonia-treated microporous carbon (a), as compared to diffraction patterns of several iron nitrides (b), carbides (c), and metallic iron phases (d). Reference data were taken from the JCPDS database (released in 1985).

The diffraction patterns of the iron nitrides appearing in (b) are: (7) Fe_2N, JCPDS 06-0656; (Δ) Fe_3N, JCPDS 076-0091; and (Y) Fe_4N, JCPDS 077-2006. The diffraction patterns of the two iron carbides shown in (c) are: (●) Fe_3C, JCPDS 06-0686; and (○) Fe_3C, JCPDS 23-1113. Finally, (d) displays two iron metal phases: (■) α-Fe, JCPDS 06-0696; and (□) ε-Fe, JCPDS 34-0529.

While the particles of iron nitride are visible by TEM at all Fe-contents (see Fig. 3 of the main manuscript), the X-ray diffractograms only show signs of them in the catalysts with Fe-loadings ≥ 0.84 wt% Fe. It is at these higher Fe-concentrations that not only the concentration but also the size of the particles of iron nitride are large enough to be detected by XRD. This result confirms our observation by TEM that, as the Fe-loading of the catalysts increases, the particles of Fe-nitride become more abundant and larger. Moreover, comparing the diffractograms with the reference data of Fe_3C (c) and metallic iron species (d) enables us to exclude the presence of any large particles of these phases in our catalysts. Both carbide and metallic iron are often found in porphyrin-based catalysts heat-treated in an inert atmosphere at high temperature (> 600 °C).[3-6]

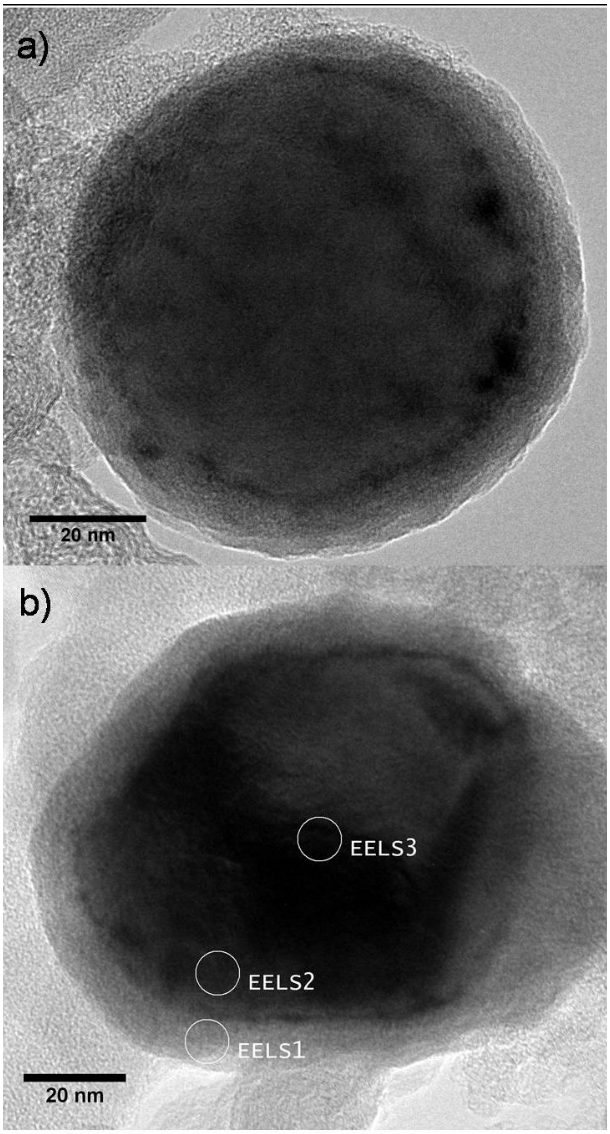

c)

	EELS1	EELS2	EELS3
Element	Content / at%		
Fe	45	60	66
N	18	28	28
O	37	12	6

Figure S4: TEM images of typical surface-oxidized iron nitride nanoparticles in catalysts with (a) 0.84 wt% Fe and (b) 1.55 wt% Fe. In (c) the atomic contents as measured at the spots EELS 1 to EELS 3 are given for the iron nitride nanoparticle shown in (b).

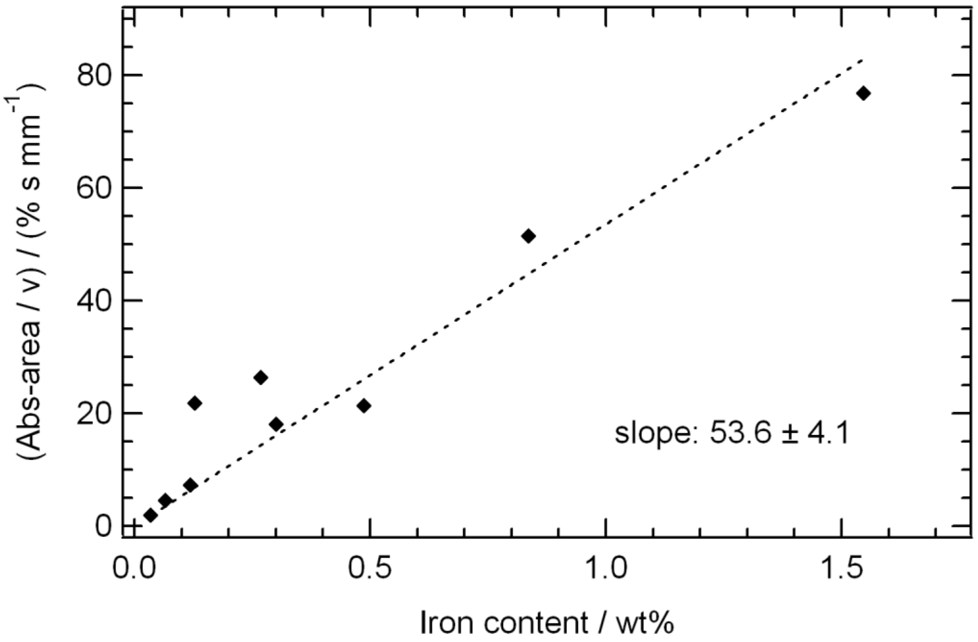

Figure S5. Integral of the absorption area of each Mössbauer spectrum as a function of the iron content in the corresponding samples.

The Debye-Waller factor describes the probability that an iron-57 site will resonantly absorb a γ-ray emitted by the ^{57}Co source. In order to attain this resonant absorption, the recoil of the absorbing nucleus has to be low enough to allow the nucleus to come back to its original position within the lifetime of the excited state. Among others, this factor depends on the bond-properties of the investigated modifications. The linear correlation between absorption area and iron content shown above allows us to assume that there are no significant differences in the absorption probability of the different iron species in these Fe/N/C-catalysts. Since there is a good agreement between the samples, it seems justified to calculate the iron contents related to each Mössbauer site applying Equation 7 of the main manuscript.

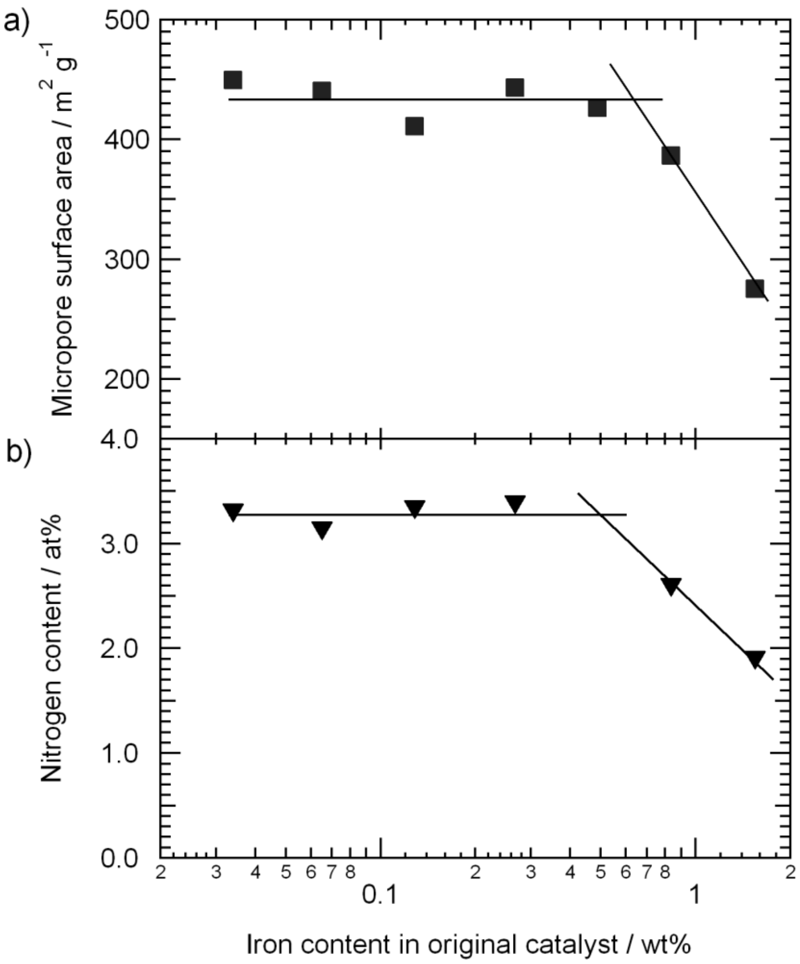

Figure S6. Evolution of the catalysts' micropore surface area (a) and nitrogen content (b) with increasing iron content. Bulk nitrogen content was determined by combustion analysis and bulk iron content by neutron activation analysis.

A possible relation between the adsorption of iron acetate and the lower microporosity and ORR-activity of the catalyst with > 0.6 wt% Fe.

In the first step of the catalyst synthesis, when carbon black and ferrous acetate salt are poured into deionized water, the highly soluble acetate promptly dissociates into Fe^{2+} and $H_3C{-}COO^-$ ions. Upon subsequent drying at 85°C, the liquid in this suspension evaporates and the molecules of iron^{II} acetate reform, adsorbing onto the predominantly apolar surface of the carbon with their methyl-groups ($H_3C{-}$) oriented towards the carbon's surface. Each methyl group occupies ≈ 0.25 nm^2,[7] and so each adsorbed molecule of iron^{II} acetate has a footprint of ≈ 0.5 nm^2 on the carbon surface. Considering that our pristine carbon has a specific surface area of 72 m^2·g^{-1}, one can estimate that a close-packed monolayer of adsorbed salt corresponds to a metal content of 1.34 wt% Fe. When the weight loss in the subsequent NH_3-pyrolysis is taken into consideration (i.e. 30-35%), this monolayer of impregnated iron acetate translates into a catalyst with ~ 2.1 wt% Fe.

In this close-packed, monolayer configuration, the lack of free space in between the molecules of ferrous acetate could easily result in the fast agglomeration of the iron at the very beginning of the heat-treatment. Too much metallic iron may indeed favour: (i) the decomposition of NH_3, lowering therefore the rate of pore formation and integration of N-bearing functionalities that cause the drop of the catalysts' micropore suface area and nitrogen content, respectively; and (ii) the production of large iron nitride particles that divert part of the iron from producing FeN_4-like sites. Interestingly, according to Figure S4, the iron content at which the micropore surface area and the nitrogen concentration begin to decrease is ~ 0.6 wt% Fe. This corresponds to ~ 1/3 monolayer of iron acetate adsorbed on the pristine carbon. Therefore, it seems that, in order to avoid this agglomeration and the subsequent decrease of microporosity, nitrogen content and number of active sites, a maximum of ~ 30% of the surface of the carbon can be occupied by molecules of iron acetate.

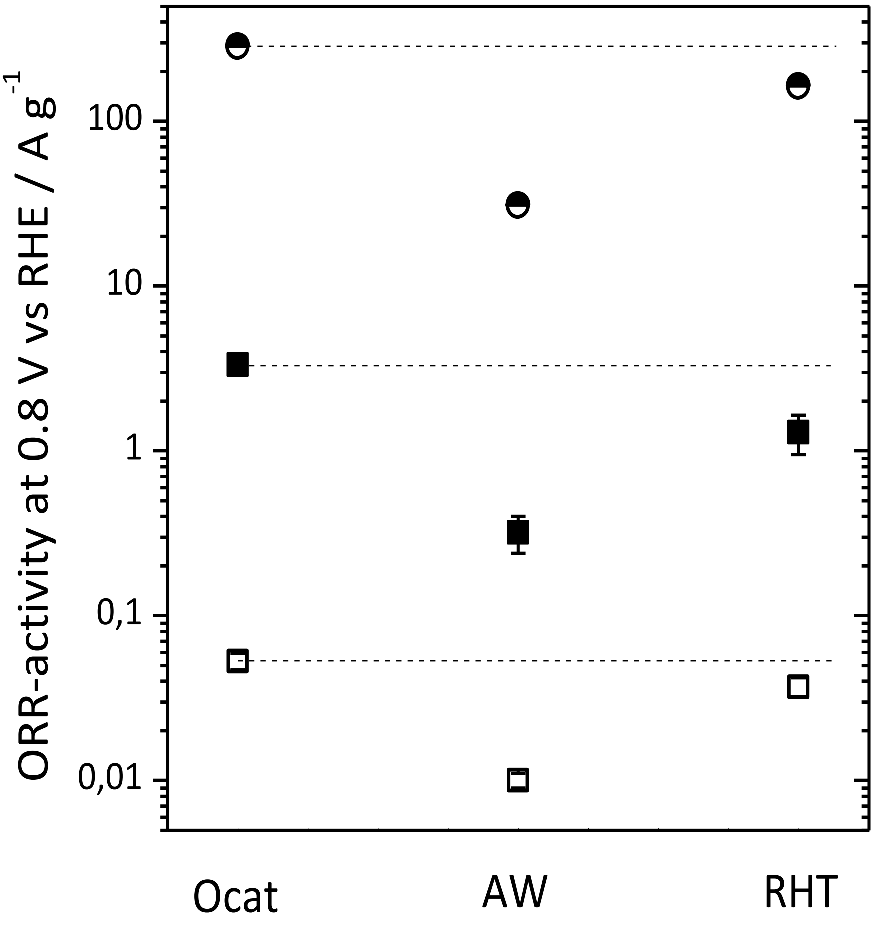

Figure S7. Comparison of the ORR-activities measured by RDE for the catalyst containing ~ 0.27 wt% Fe (full squares) and the microporous, N-containing but Fe-free carbon prepared by pyrolysis in NH_3 (empty squares), for the as-prepared materials (Ocat) and their acid-washed (AW) and re-heat-treated derivatives (RHT, 1h in Ar at 400°C). A similar comparison is also shown (half filled circles) for the much more active Fe/N/C catalyst of reference 13 (in the main text) containing ~ 1 wt% Fe. Here the ORR activity was measured in PEM fuel cell at 0.8V vs RHE.

Figure 8: Procedure to calculate activities at 0.8V RHE / (A g^{-1}) vs the iron content / (wt% Fe) in the original catalysts assuming three hypotheses:

(i) if nitride, singlet and D3 are ORR active;
(ii) if singlet and D3 are ORR active
(iii) if only D3 is ORR active

The reference activity of Ocat5 is 3.3 A g^{-1} at 0.8V RHE.

Example of calculated activity for 0.84 wt% Fe content if nitride, singlet and D3 are ORR active:
Calculated activity =
[contribution of the nitride + contribution of the singlet + contribution of D3] x reference activity =
[(0.24 x 0.179/).0080) + (0.32 x 0.52/0.13) + (0.44 x 0.035/0.019)] x 3.3 A g^{-1} =
[0.54 + 1.28 + 0.81] x 3.3 A/g = **8.7 Ag^{-1}**.
Here:

0.24	is the fraction of the activity attributed to the nitride in Ocat6 in Figure 6a.
0.179	is the wt% Fe attributed to the iron nitride for the catalyst with 0.84 wt% Fe in Figure 4e (see Table S1).
0.080	is the wt% Fe attributed to the iron nitride for the reference catalyst (0.27 wt% Fe) in Figure 4e.
0.32	is the fraction of the activity attributed to the singlet in Ocat6 in Figure 6a.
0.52	is the wt% Fe attributed to the singlet for the catalyst with 0.84 wt% Fe in Figure 4f.
0.13	is the wt% Fe attributed to the singlet for the reference catalyst (0.27 wt% Fe) in Figure 4f.
0.44	is the fraction of the activity attributed to D3 in Ocat6 in Figure 6a.
0.035	is the wt% Fe attributed to D3 for the catalyst with 0.84 wt% Fe in Figure 4d.
0.019	is the wt% Fe attributed to D3 for the reference catalyst (0.27 wt% Fe) in Figure 4d.

Example of calculated activity for 0.84 Fe content if singlet and D3 are ORR active:
Calculated activity =
[contribution of the singlet + contribution of D3] x reference activity =
[(0.32 x 0.52/0.13) + (0.68 x 0.035/0.019)] x 3.3 A g^{-1} =
[1.28 + 1.25] x 3.3 A/g = **8.4 A g^{-1}**.
Here:

0.32	is the fraction of the activity attributed to the singlet in Ocat6 in Figure 6a.
0.52	is the wt% Fe attributed to the singlet for the catalyst with 0.84 wt% Fe in Figure 4f.
0.13	is the wt% Fe attributed to the singlet for the reference catalyst (0.27 wt% Fe) in Figure 4f.
0.68	is (0.44 + 0.24), the total fraction of the activity attributed to D3 in Ocat6 in Figure 6a.
0.035	is the wt% Fe attributed to D3 for the catalyst with 0.84 wt% Fe in Figure 4d.
0.019	is the wt% Fe attributed to D3 for the reference catalyst (0.27 wt% Fe) in Figure 4d.

Example of calculated activity for 0.84 Fe content if only D3 is ORR active:
Calculated activity =
[contribution of D3] x reference activity =
[(1.00 x 0.035/0.019)] x 3.3 A g^{-1} =
[1.85] x 3.3 A/g = **6.07 A g^{-1}**.
Here:

1.00	is (0.68 + 0.32), the total % of the activity attributed to D3 in Ocat6 in Figure 6a.
0.035	is the wt% Fe attributed to D3 for the catalyst with 0.84 wt% Fe in Figure 4d.
0.019	is the wt% Fe attributed to D3 for the reference catalyst (0.27 wt% Fe) in Figure 4d.

Table S1: ORR activity at 0.8V RHE of the catalysts in Figure 4a and iron contents (wt%) for the various Fe species in the same catalysts Figure 4b to 4e.

Fe-cont / wt%	ORR-act. (0.8V)	Sing / wt%	FexN / wt%	D1 / wt%	D2 / wt%	D3 / wt%
0.03	0.4	0	0.006	0.015	0.008	0.005
0.07	0.7	0	0.017	0.024	0.011	0.013
0.13	1.9	0	0.074	0.028	0.013	0.013
0.27	3.3	0.13	0.080	0.018	0.021	0.019
0.49	3.2	0.32	0.107	0.062	0.023	0.022
0.84	5.9	0.52	0.179	0.075	0.030	0.035
1.55	0.7	0.70	0.690	0.113	0.019	0.014

Supplementary bibliography

1. E.Kuzmann, A. Nath, V. Chechersky, S. Li, Y.Wei, X. Chen, J. Li, Z. Homonnay, M. Gal, V. K. Garg, Z. Klencsar and A. Vertes, *Hyperfine interactions*, 2002, **139/140**, 631-639.
2. F. Charreteur, F. Jaouen, S. Ruggeri and J.P. Dodelet, *Electrochimica Acta*, 2008, **53**, 2925-2938.
3. J. Blomquist, H. Lang, R. Larsson and A. Widelöv, *J. Chem. Soc., Faraday Trans*., 1992, **88,** 2007-2011.
4. S. L. Gojkovic, S. Gupta and R. F. Savinell, *Journal of the Electrochemical Society,* 1998, **145,** 3493-3499.
5. M. R. Tarasevich and K. A. Radyushkina, *Mater. Chem. & Phys.*, 1989, **22**, 477-502.
6. U. I. Kramm, I. Herrmann, S. Fiechter, G. Zehl, I. Zizak, I. Abs-Wurmbach, J. Radnik, I. Dorbandt and P. Bogdanoff, *ECS Transactions*, 2009, **25**, 659-670.
7. W. X. Lu, H. L. Zhou, P. S. He and W. H. Guo *This Solid Films*, 2000, **365**, 67-71.